Experimental Investigation and Optimizing the Parameters of a Solar Air Heater Having Broken Arc-Shaped Ribs Using Hybrid Entropy-VIKOR Technique

Sheetal Kumar Jain
School of Refrigeration and Air-Conditioning Skills,
Bhartiya Skill Development University,
Jaipur 302037, Rajasthan, India
e-mail: sheetal.kumar@ruj-bsdu.in

Rohit Misra[1]
Department of Mechanical Engineering,
Ajmer Engineering College,
Ajmer 305002, Rajasthan, India
e-mail: rohiteca@rediffmail.com

Ghanshyam Das Agrawal
Department of Mechanical Engineering,
Malaviya National Institute of Technology,
Jaipur 302017, Rajasthan, India
e-mail: gdagarwal.mech@mnit.ac.in

In this article, thermal performance of a solar air heater (SAH) having broken arc-shaped ribs has been investigated experimentally, and then, performance parameters have been optimized. Study reveals that the use of artificial roughness enhances both heat transfer rate and pumping power requirement, and hence, the overall performance of solar air heater increases. Thus, it is imperative to optimize the performance-defining criteria viz. Nusselt number enhancement ratio, friction factor enhancement ratio, and thermohydraulic performance parameter, to propose an optimal set of flow and roughness parameters. The hybrid entropy-VIKOR technique has been employed to outline the optimal set of parameters using performance-defining criterions, to obtain maximum profit with the minimum incurred cost. The optimal set of parameters attained using entropy-VIKOR approach among all the alternatives is as follows: relative gap width = 4, relative roughness pitch = 10, and arc angle = 45 deg at Reynolds number = 9000.
[DOI: 10.1115/1.4055297]

Keywords: optimization, solar air heater, VIKOR, MCDM technique, broken arc-shaped ribs, heat transfer

1 Introduction

The environment concern and exhaustible energy sources have accelerated the use of clean and green energy globally. The efficient technologies to harness energy from green energy resources are also progressing year by year throughout the world. Solar energy, no doubt, with its abundant inherent energy leads among the green energy resources for exploration and on its extensive utilization. The installation of solar thermal collectors, i.e., water collectors and air collectors, is also progressing worldwide. But as per IEA SHC—Solar Heat Worldwide 2020 report, the installation of solar air heating systems (air collectors) was limited to only 0.2% of the total number of solar thermal collectors installed in the year 2018. Transformation of solar energy into thermal energy can be achieved using heating of a fluid through solar air heater (SAH). The solar air heater used for space heating and drying applications is not accepted widely due its poor thermal performance [1–5]. Formation of laminar sublayer leads to poor thermohydraulic performance of SAH. The thermohydraulic performance of SAH may be enhanced by employing a variety of heat transfer improvement methods. One of the methods of augmenting the performance of SAH is to have absorber plate (AP) with artificial roughness in the form of ribs and baffles. The ribs enhance the heat transfer rate as they result into an increase in surface area and promote turbulence in flow, which in turn disrupts the laminar sublayer [6–8]. Researchers keep on investigating an optimal artificial roughness geometry, which can deliver enhanced thermohydraulic performance of SAH [9–13].

Roughness parameters greatly influence the thermohydraulic performance of SAH. Researchers focus on optimizing the parameters to propose a group of parameters that will lead to maximum heat transfer rates with minimum escalation in pumping power requirement. The process of exploring the combination of optimized and interdependent set of parameters is really cumbersome. Hence, a simple, systematic, and practical approach is required to select and specify the system parameters that lead to an overall best performance of the system. Kumar [14] studied the performance of SAH whose duct had concave dimple-shaped roughness, and Nu and f were reported to be much higher for duct having roughness on three sides than for the duct having roughness on only one side. Promthaisong and Eiamsa-ard [15] performed a simulation study to explore the heat transfer and friction attributes of wavy triangular ribs attached on the AP. The study reported that the wavy triangular ribs induced the vortex flows, which destructed the laminar sublayer and resulted into higher heat transfer rate. Kumar et al. [16] also carried out a computational fluid dynamics simulation and investigated the heat transfer and flow attributes in a SAH having a triangular cross-sectional passage, whose AP was roughened with square-shaped ribs. Singh et al. [17] experimentally investigated a finned wire mesh packed bed SAH and reported maximum thermal and thermohydraulic efficiency of 93% and 80% at a mass flowrate ($\dot{m}$) of 0.03 kg/s and 0.023 kg/s, respectively. Ahmad et al. [18] numerically investigated the thermohydraulic performance of a SAH having equilateral prism-shaped ribs and reported the maximum value of thermohydraulic performance factor as 3.41.

The multiple criteria decision-making (MCDM) [19,20] approaches are quantifiable methods for resolving difficulties including variety of alternatives. Entropy-VIKOR technique is one of the widely exercised techniques applied as MCDM approach, and this hybrid technique provides a compromised solution after ranking the alternatives. The compromised solution offered is practical one and closely approximates an ideal solution.

[1]Corresponding author.

Contributed by the Solar Energy Division of ASME for publication in the Journal of Solar Energy Engineering: Including Wind Energy and Building Energy Conservation. Manuscript received December 13, 2020; final manuscript received August 12, 2022; published online September 26, 2022. Assoc. Editor: Kashif Nawaz.

Several researchers have conducted studies involving entropy-VIKOR method to solve problems, which include a variety of alternatives and for which an optimal set of performance-defining criterion (PDC) is required. Ahlawat et al. [21] employed VIKOR technique to obtain the best friction composite from the developed composites on the basis of considered criterion chosen for performance evaluation. First, entropy technique was applied to determine the mass of each PDC, and further, VIKOR technique was applied to rank them. Zheng and Wang [22] used the VIKOR technique to grade the renewable energy systems in tourist resorts; weightage of selected criterion and subcriterion were determined. In a study by Mojaver et al. [23], VIKOR technique was used to select the optimal biomass based on the performance criterion. Different biomasses were considered in the study such as eucalyptus, groundnut shell, and sugarcane bagasse. To evaluate the performance; energy, exergy, and environmental factors were taken into account. Li et al. [24] applied LDVIKOR (later defuzzification VIKOR) technique for selection of machine tools as machine tools highly affect the efficacy of a product. Results obtained were in great agreement with the real factory ranking of tools. Chou et al. [25] employed VIKOR technique to evaluate the performance level of women in science and technical field. Two criteria considered were government sector and higher education sector. Das et al. [26] used the classic VIKOR method to grade the recognized threats in actions connected with process, product, and services. Maximum group utility and minimum regret concepts were assimilated. Demirel et al. [27] used the VIKOR technique to figure out the most satisfactory stabilization arrangement on yachts to reduce the mobility due to the forces to which yacht is imparted with. Narayanamoorthy et al. [28] used entropy-based VIKOR technique to choose a right robot for the particular application from the wide variety of options available as selecting the suitable robot is a very difficult task, and these robots are used to perform perplexed and risky tasks accurately. Rani et al. [29] employed VIKOR technique for choosing renewable energy technologies, and it was concluded that PF-VIKOR (Pythagorean Fuzzy VIKOR) is an efficient method to assess renewable technologies as it is a tedious task for the deciding person. Shemshadi et al. [30] applied VIKOR technique to grade the suppliers for a firm as the firm is affected most by its supplying partners. Conflicting and incomparable criteria were taken into account. Sun et al. [31] proposed extended VIKOR technique to obtain compromise solutions envisaging hybrid characteristics for the optimized decision-making to assure fast and secure supply restoration of power to the end users. Wang et al. [32] created a multicriteria decision-making framework for the risk assessment of construction project with picture fuzzy information, and they also integrated the VIKOR with picture fuzzy normalized projection model to validate the model. In a study by Sharma et al. [33], VIKOR technique was employed to get an optimal parameter set for SAH having obstructions in the form of discrete V-ribs to develop an efficient system, which can meet the performance-defining criterion. Gao et al. [34] used VIKOR to prioritize projects of concrete bridge damaged by corrosion so that the level of attention a project need can be inferred. A new ranking system technique using weighted VIKOR is also introduced by the author.

The authors of this article investigated the relevancy of the hybrid entropy-VIKOR technique [35–38] for solar air heater having broken arc-shaped ribs. An experimental analysis has been conducted to determine the thermal performance, which will be further used in assessing the performance-defining criteria, to satisfy the applicability. In the present study, the authors are discussing the suggested methodology to determine the optimum design parameters with the purpose of obtaining maximum overall thermal performance under given working circumstances. The Nusselt number enhancement ratio (NNER), friction factor enhancement ratio (FFER), and thermohydraulic performance parameter (THPP) are used to identify the optimal design set. In this optimization technique, the entropy method determines the weight of each PDC, and the VIKOR method ranks each alternative as per VIKOR index.

2 Description of Experimental Setup

2.1 Investigation Setup. The indoor experimental setup is designed and fabricated consistent with the standards to study the influence of broken arc-shaped ribs on heat transfer and fluid flow characteristics of SAH duct as per ASHRAE standards 93–97 [39]. The rectangular duct portrays a SAH duct with three smooth surfaces and one rough surface causing turbulence for the air flow. Figure 1 shows the photographic view of the designed experimental setup. The aspect ratio (W/H) and hydraulic diameter (Dh) of the duct are maintained at 10:1 and 54.54 mm, respectively. The length of the entry and exit section was taken to be $5\sqrt{W*H}$ and $2.5\sqrt{W*H}$, respectively, as per the guidelines of ASHRAE standards 93–97 [39]. A cross section of the duct is 300 mm × 30 mm, and its length is 2900 mm. Duct has three distinct sections, namely, an inlet section, test section, and an exit section having a length of 500 mm, 2000 mm, and 300 mm, respectively. To get uniform temperature of the fluid at the outlet of the exit section, a mixing zone of length of 100 mm with perforated baffles is provided to ensure proper mixing of heated air molecules. Figure 1 depicts the 3D model of test setup employed in investigation. The AP of SAH was made up of galvanized iron sheet, and artificial roughness was pasted on the underside of it. The upper surface of the AP was painted black so as to increase its absorptivity. A

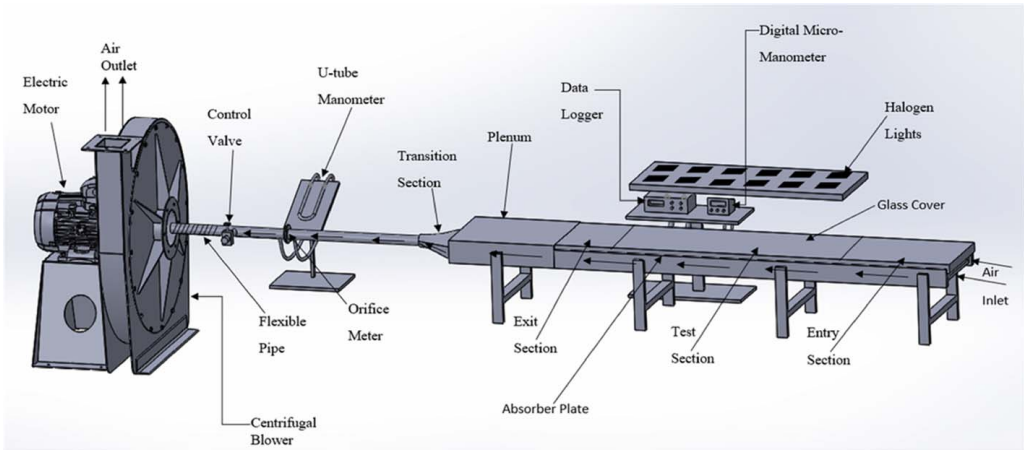

Fig. 1 3D model of experimental test rig

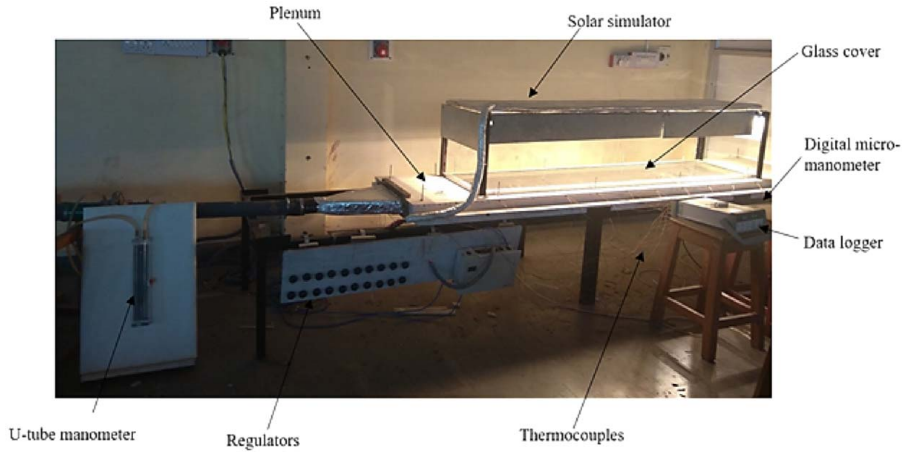

Fig. 2 Experimental test rig setup

thick glass sheet of 5 mm was used as a cover plate over the AP to confine the insolation.

Heating of the AP was accomplished by concentrating the radiations on it by means of a solar simulator. The solar simulator comprises 20 halogen lamps mounted inside a reflecting panel, which directs the radiation to impinge on the AP, as shown in Fig. 2. The supply of the electric current to each of the halogen lamp was independently regulated to attain a uniform heat flux of 1000 W/m^2 over the AP. Air was sucked through the duct using a centrifugal blower, and the air flow velocity was regulated by running the blower at different rpm by means of a dimmerstat. A pyranometer was used to measure the intensity of radiation falling on the AP. A well-calibrated orifice meter along with a U-tube manometer was employed to measure the mass flowrate of air through the duct. All joints of duct, inlet section, test section, exit section, and pipes are thoroughly checked for any leakage before starting the experiment every time. The flowrate of air in the duct has been maintained for about 30 min to ensure the quasi-steady-state condition established for each flowrate. The pressure drop across the test section was measured with the help of digital micro-manometer. Temperature of air and AP were measured with the help of T-type thermocouples, which were connected to a data acquisition system. Figure 3 represents the position of 33 thermocouples (one thermocouple at inlet section (T_i), 27 thermocouples on AP (T_{p1} to T_{p27}), and 5 thermocouples at outlet section (T_{o1}–T_{o5})) mounted for measuring the temperature. Thermal properties of air are considered to be constant.

2.2 Range of Geometrical and Flow Parameters. Figures 4(*a*) and 4(*b*) represent the schematic and actual representation of the roughness, respectively, i.e., broken arc-shaped ribs and related geometrical parameters. In the current study, the thermohydraulic attributes of broken arc-shaped ribs have been examined by varying geometrical and flow parameters of roughness. The range of roughness and flow parameters that are considered in the present investigation are listed in Table 1.

3 Data Reduction

Experimentally observed values of temperature of AP at 27 points and temperature of air at the inlet and outlet section were used for determining the mean temperature of absorber plate (T_{pm}) and mean temperature of air (T_{fm}) in the test section as follows:

Mean absorber plate temperature, expressed in Eq. (1), is the average of temperatures given by 27 thermocouples:

$$T_{\mathrm{pm}} = \frac{T_{\mathrm{p1}} + T_{\mathrm{p2}} + T_{\mathrm{p3}} + \ldots\ldots\ldots\ldots\ldots T_{\mathrm{p27}}}{27} \tag{1}$$

The average air temperature (T_{fm}) across the test section is given as follows:

$$T_{fm} = \frac{T_i + T_o}{2} \tag{2}$$

where T_i is the inlet air temperature.

The outlet air temperature (T_o) is calculated as follows:

$$T_o = \frac{T_{o1} + T_{o2} + T_{o3} + T_{o4} + T_{o5}}{5} \tag{3}$$

The mass flowrate of air is expressed by the following equation:

$$\dot{m} = C_d A_o \left[\frac{2\,\rho_a(\Delta P_o)}{1-\beta^4}\right]^{0.5} \tag{4}$$

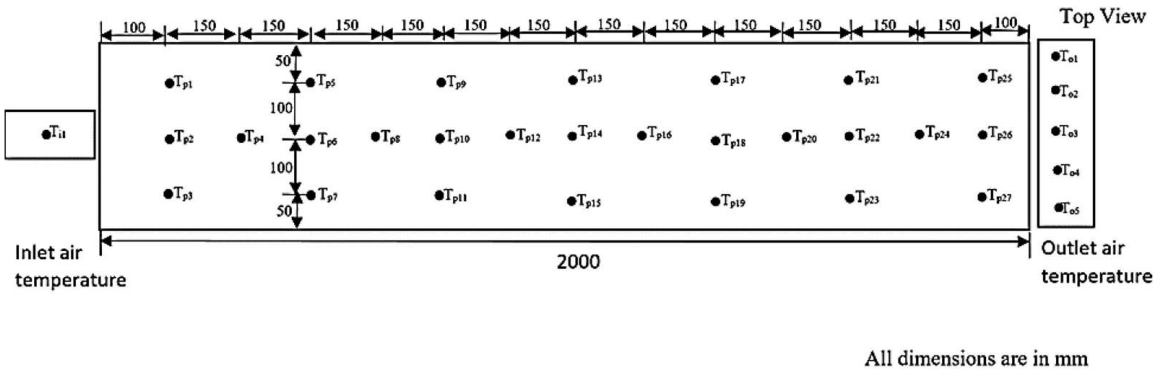

Fig. 3 Position of thermocouples on absorber plate

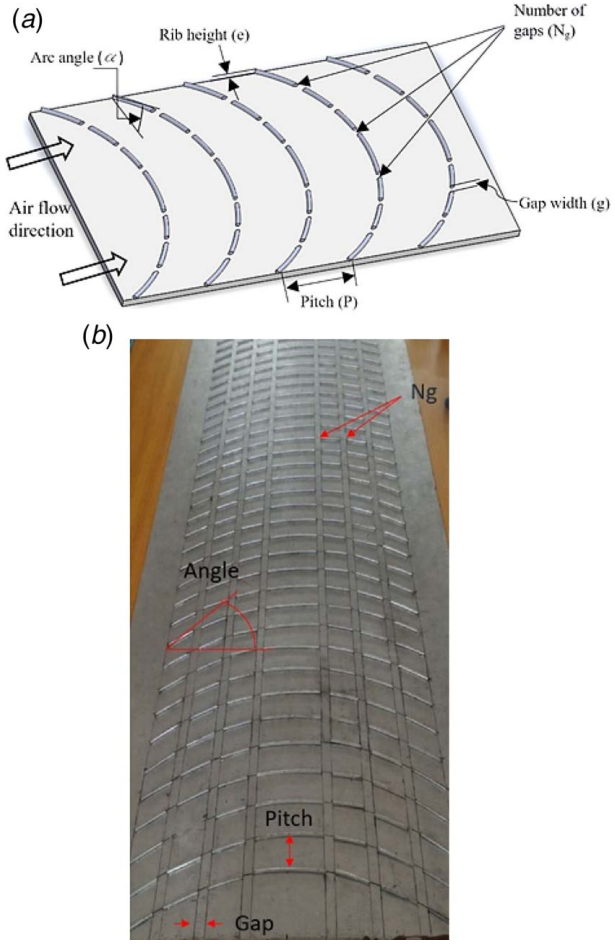

Fig. 4 (*a*) Schematic and (*b*) actual representation of absorber plate and geometric parameters

Table 1 Range of geometrical and flow parameters

Sr. no.	Parameters	Range
1	Arc angle (α)	45 deg and 60 deg
2	Reynolds number (Re)	3000–18,000
3	Relative gap width (g/e)	2, 3, 4, and 5
4	Relative roughness pitch (P/e)	8, 10, 12, and 14

Heat transferred to the air is given as follows:

$$Q_u = \dot{m} C_p \, (T_o - T_i) \tag{5}$$

The convective heat transfer coefficient is derived from the following equation as follows:

$$h = \frac{Q_u}{A_p (T_{\text{pm}} - T_{\text{fm}})} \tag{6}$$

The Nusselt number (Nu) and friction factor (f) are determined as follows:

$$\text{Nu} = \frac{hD}{k} \tag{7}$$

$$f = \frac{\Delta P_d \times D}{2\rho_a \times L \times V^2} \tag{8}$$

The NNER and FFER are represented by

$$\text{NNER} = \left(\frac{\text{Nu}_r}{\text{Nu}_s}\right) \tag{9}$$

$$\text{FFER} = \left(\frac{f_r}{f_s}\right) \tag{10}$$

The THPP [40,41] is given as follows:

$$\text{THPP} = \left(\frac{\text{Nu}_r}{\text{Nu}_s}\right) \Big/ \left(\frac{f_r}{f_s}\right)^{1/3} \tag{11}$$

4 Optimization Methodology

A MCDM approach deals with the ranking and the selection of the optimal choice from a set of input. The MCDM approach provides a vigorous framework for material determination in perspective of the evaluation of various conflicted criterion. VIKOR approach is among the popular MCDM techniques that provide ranking to alternatives and establish the compromised solution, which approximates the ideal solution. Because of its wide application, hybrid entropy-VIKOR technique has been utilized in optimization of roughness and flow parameters of broken arc-shaped ribs. The assessment procedure of hybrid entropy-VIKOR technique is explained in the flowchart as portrayed in Fig. 5. The methodology can be summed up in three phases as follows:

Phase-I: Elementary structure
Phase-II: Entropy method
Phase-III: VIKOR method

4.1 Phase-I: Elementary Structure. In this primary phase, the number of alternatives and the PDCs are identified from experimentation, and concurrently, a decision matrix ($D_{M\times N}$) is constructed. The decision matrix thus formed has an order of $M \times N$, where the number of alternatives are represented by "M," while N indicates the different PDCs. The decision matrix is presented in Eq. (12) as follows:

$$D_{M\times N} = \begin{bmatrix} d_{11} & d_{12} & \dots & d_{1N} \\ d_{21} & d_{22} & \dots & d_{2N} \\ \vdots & \vdots & \dots & \vdots \\ d_{M1} & d_{M2} & \dots & d_{MN} \end{bmatrix} \tag{12}$$

In the matrix, each element (d_{ij}) corresponds to actual experimental value of the ith alternative for the jth criterion. Subsequently, the profit $(d_{ij})_{\max}$ and cost criterions $(d_{ij})_{\min}$ are determined as per Eqs. (13) and (14).

$$(d_{ij})_{\max} = i^{\max} d_{ij} = \max\,[d_{ij},\, i = 1, 2 \dots M] \tag{13}$$

$$(d_{ij})_{\min} = i^{\min} d_{ij} = \min\,[d_{ij},\, i = 1, 2 \dots M] \tag{14}$$

4.2 Phase-II: Entropy Method. In this phase, the entropy method is used in computation of the weight of various criterions (ω_j). To calculate the weight of criterions, first, projection value (π_{ij}) of each alternative is calculated using Eq. (15), which is further used to calculate the entropy of each criterion (ε_j). Finally, the criterion weight is calculated using Eq. (18).

$$\pi_{ij} = \frac{d_{ij}}{\sum_{i=1}^{M} d_{ij}} \tag{15}$$

$$\varepsilon_j = -\varsigma \sum_{j=1}^{N} \pi_{ij} \ln(\pi_{ij}) \tag{16}$$

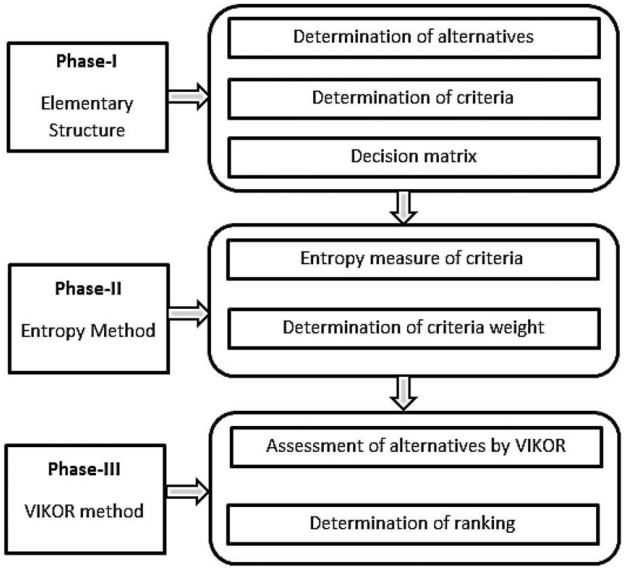

Fig. 5 Flowchart to determine the compromise solution using hybrid entropy-VIKOR technique

$$\varsigma = \frac{1}{\ln(M)} \tag{17}$$

$$\omega_j = \frac{\psi_j}{\sum_{j=1}^{N} \psi_j} \tag{18}$$

where π_{ij} is the projection value, ε_j is entropy of each criteria, ς_i s amendment constant, ψ_j is the dispersion value, and ω_j is weight of each criteria.

4.3 Phase-III: VIKOR Method. In this method, the identified alternatives are evaluated, and a ranking is assigned to each alternative. To determine the ranking, first, utility measure ($\hbar_i$) and regret measure (λ_i) values are computed using Eqs. (19)–(21).

$$\hbar_i = \sum_{j=1}^{N} \frac{\omega_j[(d_{ij})_{\max} - d_{ij}]}{[(d_{ij})_{\max} - (d_{ij})_{\min}]} \text{ if } j \text{ is profit criteria} \tag{19}$$

$$\hbar_i = \sum_{j=1}^{N} \frac{\omega_j[d_{ij} - (d_{ij})_{\min}]}{[(d_{ij})_{\max} - (d_{ij})_{\min}]} \text{ if } j \text{ is cost criteria, } j = 1, 2, \ldots M \tag{20}$$

$$\lambda_i = \left\{ \frac{\omega_j[(d_{ij})_{\max} - d_{ij}]}{[(d_{ij})_{\max} - (d_{ij})_{\min}]} \right\} j = 1, 2, \ldots N \tag{21}$$

Finally, the VIKOR index (θ_i) is calculated as per Eq. (22). The VIKOR index is used in the ranking of each alternative. The alternative with a least value of θ_i is given first ranking, and similarly, each alternative is ranked in the ascending order of θ_i.

$$\theta_i = \nu\left(\frac{(\hbar_i - \hbar_i^-)}{(\hbar_i^+ - \hbar_i^-)}\right) + (1-\nu)\left(\frac{(\lambda_i - \lambda_i^-)}{(\lambda_i^+ - \lambda_i^-)}\right) \tag{22}$$

where ν = weight given to maximum value of utility, $(1-\nu)$ = weight given to individual regret, and $\hbar_i^+$, $\hbar_i^-$, λ_i^+, and λ_i^- = maximum and minimum values of utility and regret measure.

Table 2 Experimentally identified parametric combinations

Alternatives	Re	*g/e*	*P/e*	α
A-1	9000	2	8	60 deg
A-2	9000	2	10	60 deg
A-3	9000	2	12	45 deg
A-4	9000	2	14	45 deg
A-5	9000	3	8	60 deg
A-6	9000	3	10	60 deg
A-7	9000	3	12	45 deg
A-8	9000	3	14	45 deg
A-9	9000	4	8	45 deg
A-10	9000	4	10	45 deg
A-11	9000	4	12	60 deg
A-12	9000	4	14	60 deg
A-13	9000	5	8	45 deg
A-14	9000	5	10	45 deg
A-15	9000	5	12	60 deg
A-16	9000	5	14	60 deg

5 Results and Discussion

5.1 Experimental Results. The performance of rectangular SAH duct having arc-shaped broken ribs as artificial roughness is determined experimentally by varying geometrical and flow parameters as listed in Table 2. The evaluated values of NNER, FFER, and THPP for 16 parametric combinations are listed in Table 3. Also, the values of NNER and FFER for each alterative are plotted graphically in Fig. 6(*a*), while values of THPP for each alterative are plotted graphically in Fig. 6(*b*).

It can be observed from the experimental outcomes that arc angle, relative roughness pitch, and relative gap width of broken arc-shaped ribs have a considerable effect on heat transfer and frictional characteristics or PDCs (NNER, FFER, and THPP). It is observed that Nusselt number [22,32] increases with an increase in the relative gap width from 2 to 4 and attains a highest value at $g/e = 4$ and afterward it decreases. The reason can be ascribed that as the gap width increases, there is a much wider passage for the secondary flow to pass through and to create turbulence in the primary flow, resulting in enhanced heat transfer. When *g/e* is further increased, Nu is noticed to have a decreasing trend. As the gap width is increased further, it results in the secondary flow to deaccelerate, which results in the reduced heat transfer rate. The frictional characteristics also follows the same trend, and it first increases up to $g/e = 4$ and then decreases. The reason can be attributed that as the gap width increases, the secondary flow escalates the turbulence level in the flow, which obstructs the flow of fluid,

Table 3 Experimental outcomes of NNER, FFER, and THPP corresponding to each alternative

Alternatives	NNER	FFER	THPP
A-1	2.264	2.319	1.711
A-2	2.366	2.006	1.876
A-3	2.258	2.058	1.775
A-4	2.155	2.216	1.653
A-5	2.477	2.670	1.785
A-6	2.588	2.657	1.869
A-7	2.470	2.624	1.791
A-8	2.357	2.751	1.682
A-9	2.451	2.986	1.702
A-10	2.562	1.912	2.064
A-11	2.611	2.195	2.009
A-12	2.491	2.402	1.860
A-13	2.437	2.527	1.789
A-14	2.547	2.532	1.868
A-15	2.595	2.731	1.857
A-16	2.476	2.874	1.742

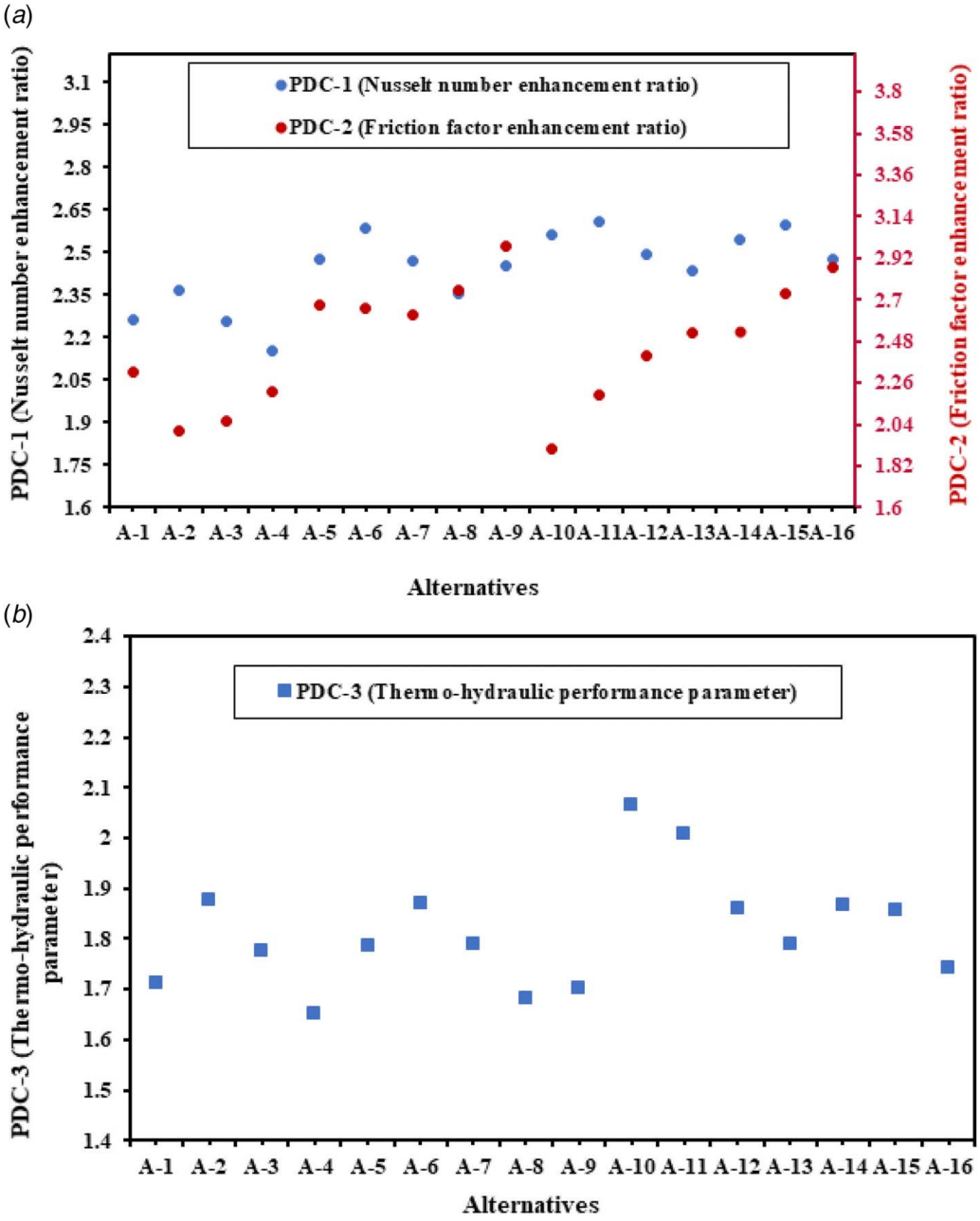

Fig. 6 (*a*) Plot of NNER and FFER variation corresponding to each alternative and (*b*) plot of THPP variation corresponding to each alternative

and hence, the pressure drop increases. But, when *g*/*e* is increased further, the gap size becomes relatively larger so that air passes easily without any obstruction, and therefore, the friction factor reduces. As relative roughness pitch increases from 8 to 10, it is noticed that Nu increases, but afterward it shows a decreasing trend. Also, the hydraulic attributes follow the same trend as Nu. The reason for this can be attributed to the fact that at lower *P*/*e* values, the reattachment of primary flow does not take place as it gets detached when it jumps over the first rib, consequently reducing the mixing with the secondary flow, which results in lower pumping power requirement. As *P*/*e* increases, the flow begins to re-attach to the absorber plate in the interrib region, which enhances the turbulence, and hence, heat transfer increases while a larger drop in pressure is noticed. As *P*/*e* is increased further due to relatively larger interrib region, the boundary layer begins to develop past the reattachment position, and it reduces the heat transfer. As the arc angle is increased from 45 deg to 60 deg, heat transfer and pumping power requirement increases and the reason can be given that the primary flow gets a gradual obstruction in flow, which increases the flow velocity of the secondary flow. It increases the mixing rate and hence heat transfer increases but, due to increased turbulence, frictional losses also increase. The representation of fluid behavior over the broken arc-shaped ribs is shown in Fig. 7.

THPP expressed by Eq. (11) concurrently assesses the thermal along with hydraulic attributes inside SAH. The variation in value of THPP is dependent on NNER and FFER. It can be noted that NNER is highest at alternative A-11 and lowest at A-4. Similarly, FFER has a highest value at alternative A-9 and least value at A-10, whereas THPP is highest at A-10 and lowest at A-4. Considering the variation in PDCs due to alternatives, the hybrid entropy-VIKOR technique has been applied to determine an optimal set of alternatives, which will provide higher cost benefit in terms of augmented heat transfer and lesser frictional power requirement.

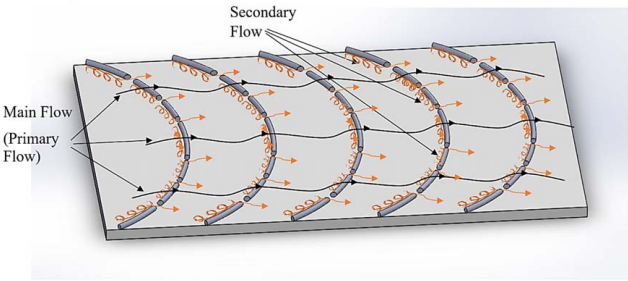

Fig. 7 Air flow pattern over the ribs

5.2 Optimization of Experimental Outcomes. The experimental outcomes of SAH having broken arc-shaped ribs have been optimized employing hybrid entropy-VIKOR technique. The following phases have been used in evaluation of the parameters.

5.2.1 Phase-I: Elementary Structure. In the first phase of optimization methodology, parametric combinations are identified from experimentation and are termed as alternatives (A-1 to A-16) and experimental outcomes viz. NNER, FFER, and THPP are termed as PDCs, i.e., C-1 for NNER, C-2 for FFER, and C-3 for THPP. A decision matrix ($D_{16\times3}$) has been constructed from identified alternatives and PDCs as represented by Eq. (23).

$$D_{16\times3} = \begin{bmatrix} 2.264(d_{11}) & 2.319(d_{12}) & 1.711(d_{13}) \\ 2.366(d_{21}) & 2.006(d_{22}) & 1.876(d_{23}) \\ \vdots & \vdots & \vdots \\ 2.476(d_{M1}) & 2.874(d_{M2}) & 1.742(d_{MN}) \end{bmatrix} \tag{23}$$

Subsequently, the profit $(d_{ij})_{\max}$ and cost $(d_{ij})_{\min}$ criterions are calculated as follows:

$$(d_{ij})_{\max} = \mathrm{i}^{\max} \quad d_{ij} = \max\begin{bmatrix} 2.611 & 2.986 & 2.064 \end{bmatrix}_{\max} \tag{24}$$

$$(d_{ij})_{\min} = \mathrm{i}^{\min} \quad d_{ij} = \min\begin{bmatrix} 2.115 & 1.912 & 1.653 \end{bmatrix}_{\min} \tag{25}$$

5.2.2 Phase-II: Entropy Method. In the second phase of entropy weight generation method, the weights of PDCs are determined. The projection values (π_{ij}), entropy (ε_j), dispersion values (Ψ_j), and weight (ω_j) have been computed using Eqs. (15)–(18). The amendment constant (ς) has been calculated using Eq. (26).

Table 4 Each alternative projected value

	Coefficient value, π_{ij}			$\pi_{ij} \times \ln(\pi_{ij})$		
	C-1	C-2	C-3	C-1	C-2	C-3
A-1	0.0579	0.0588	0.0589	−0.1650	−0.1666	−0.1669
A−2	0.0605	0.0508	0.0646	−0.1697	−0.1514	−0.1770
A−3	0.0577	0.0522	0.0611	−0.1647	−0.1540	−0.1709
A−4	0.0551	0.0562	0.0569	−0.1597	−0.1617	−0.1632
A−5	0.0633	0.0677	0.0615	−0.1748	−0.1822	−0.1715
A−6	0.0662	0.0673	0.0644	−0.1797	−0.1817	−0.1766
A−7	0.0632	0.0665	0.0617	−0.1745	−0.1802	−0.1718
A−8	0.0603	0.0697	0.0579	−0.1693	−0.1857	−0.1650
A−9	0.0627	0.0757	0.0586	−0.1736	−0.1953	−0.1663
A−10	0.0655	0.0485	0.0711	−0.1786	−0.1467	−0.1880
A−11	0.0668	0.0556	0.0692	−0.1807	−0.1607	−0.1848
A−12	0.0637	0.0609	0.0641	−0.1754	−0.1704	−0.1760
A−13	0.0623	0.0640	0.0616	−0.1730	−0.1760	−0.1717
A−14	0.0651	0.0642	0.0643	−0.1779	−0.1762	−0.1765
A−15	0.0664	0.0692	0.0640	−0.1800	−0.1848	−0.1759
A−16	0.0633	0.0728	0.0600	−0.1747	−0.1908	−0.1688
Total	*1.0000*	*1.0000*	*1.0000*	*−2.7712*	*−2.7645*	*−2.7708*

Table 5 Weight given to each criterion estimated using the entropy method

	PDCs		
Criteria	C-1	C-2	C-3
Entropy	0.9995	0.9971	0.9994
Dispersion value	0.0005	0.0029	0.0006
Weight	0.1251	0.7169	0.1580

Table 6 Utility measure, regret measure, VIKOR index, and ranking of each alternative

Alternatives	Utility measure	Regret measure	VIKOR index	Ranking
A-1	0.5026	0.2717	0.4594	6
A-2	0.2022	0.0723	0.1483	2
A-3	0.3054	0.1111	0.2341	3
A-4	0.4860	0.2029	0.4012	5
A-5	0.6500	0.5060	0.7091	12
A-6	0.5786	0.4973	0.6626	10
A-7	0.6189	0.4753	0.6697	11
A-8	0.7766	0.5600	0.8189	14
A-9	0.9000	0.7169	1.0000	16
A-10	0.0134	0.0134	0.0000	1
A-11	0.2100	0.1889	0.2356	4
A-12	0.4384	0.3271	0.4626	7
A-13	0.5640	0.4105	0.5927	9
A-14	0.5068	0.4138	0.5628	8
A-15	0.6307	0.5467	0.7271	13
A-16	0.8030	0.6421	0.8922	15

The projection values corresponding to each alternative is listed in Table 4.

$$\varsigma = \frac{1}{\ln(16)} = 0.36067 \tag{26}$$

Table 5 enlists the value of entropy, dispersion value, and weight. It can be derived from Table 5 that FFER (C-2) has the lowest value of the entropy among NNER (C-1) and THPP (C-3), and hence, it possesses more weight toward overall performance optimization.

5.2.3 Phase-III: VIKOR Method. In this phase, the values of utility measure ($\hbar_i$), regret measure (λ_i), and the VIKOR index (θ_i) have been computed using Eqs. (19)–(22) and have been listed in Table 6 along with the ranking of each alternative. The alternative having the lowest value of VIKOR index is given the first ranking, and likewise each alternative is ranked. It can be noted from Table 6 that A-10 alternative possesses the first ranking, and therefore, it is the most optimal alternative among other alternatives. The ranking of each alternative in the descending order is as follows: $A_{10} > A_2 > A_3 > A_{11} > A_4 > A_1 > A_{12} > A_{14} > A_{13} > A_6 > A_7 > A_5 > A_{15} > A_8 > A_{16} > A_9$.

6 Conclusions

In the present investigation, the performance of solar air heater having arc-shaped broken ribs has been determined experimentally, in terms of three performance criterion viz. Nusselt number enhancement ratio, friction factor enhancement ratio, and thermo-hydraulic performance parameter. An optimization study has been conducted on these three criterions using hybrid entropy-VIKOR technique. This technique includes the entropy method, which measures the weight of each criterion, and VIKOR method, which provides the ranking of alternatives. This technique offers a

compromised solution, which approximates an ideal solution. The present study concludes the following:

(1) The entropy weight generation method states that the friction factor enhancement ratio has the least value of entropy, and consequently, it has more dominating effect on the overall performance of the solar air heater having arc-shaped broken ribs compared to that of other performance-defining criteria.
(2) The VIKOR method suggests A-10 as the most optimal alternative. The ranking of each alternative follows the order as given: $A_{10} > A_2 > A_3 > A_{11} > A_4 > A_1 > A_{12} > A_{14} > A_{13} > A_6 > A_7 > A_5 > A_{15} > A_8 > A_{16} > A_9$.

On the basis of experimental investigation and using entropy-VIKOR approach optimization technique, optimal set of parameters attained among all the alternatives is as follows: relative gap width = 4, relative roughness pitch = 10, and arc angle = 45 deg at Reynolds number = 9000.Therefore, it has been concluded that hybrid entropy-VIKOR technique can be employed to solar air heaters involving multiple performance-defining criterion to provide the most optimal alternative.

Acknowledgment

The researchers are indebted to MHRD, Government of India and MNIT Jaipur for awarding financial assistance.

Conflict of Interest

There are no conflicts of interest.

Data Availability Statement

No data, models, or code were generated or used for this paper.

Nomenclature

f = friction factor
D = hydraulic duct diameter, m
H = duct height, m
L = length of test section, m
W = width of duct, mm
$\dot{m}$ = mass flowrate, kg/s
A_o = area of orifice plate, m^2
A_p = area of absorber plate, m^2
C_d = discharge coefficient
Q_u = useful heat gain, W
T_{fm} = mean temperature of fluid, K
T_i = inlet temperature of air, K
T_o = outlet temperature of air, K
T_{pm} = mean temperature of absorber plate, K
Nu = Nusselt number
ΔP_o = pressure drop across the orifice plate, Pa

Greek Symbols

α = arc angle, deg
ρ_a = density of air, kg/m^3

Subscripts

d = duct
r = roughened
s = smooth

References

[1] Cuzminschi, M., Gherasim, R., Girleanu, V., Zubarev, A., and Stamatin, I., 2018, "Innovative Thermo-Solar Air Heater," Energy Build., **158**, pp. 964–970.
[2] Ryan, D., and Burek, S. A. M., 2010, "Experimental Study of the Influence of Collector Height on the Steady State Performance of a Passive Solar Air Heater," Sol. Energy, **84**(9), pp. 1676–1684.
[3] Schnieders, J., Feist, W., and Rongen, L., 2015, "Passive Houses for Different Climate Zones," Energy Build., **105**, pp. 71–87.
[4] Shalaby, S. M., Kabeel, A. E., El-Bialy, E., and Elfakharany, M. K., 2020, "Investigation and Improvement of Thermal Performance of a Solar Air Heater Using Extended Surfaces Through the Phase Change Material," ASME J. Sol. Energy Eng., **142**(1), p. 011012.
[5] Saxena, A., and El-sebaii, A. A., 2015, "A Thermodynamic Review of Solar Air Heaters," Renewable Sustainable Energy Rev., **43**, pp. 863–890.
[6] Kumar, A., 2014, "Analysis of Heat Transfer and Fluid Flow in Different Shaped Roughness Elements on the Absorber Plate Solar Air Heater Duct," Energy Procedia, **57**, pp. 2102–2111.
[7] Karwa, R., 2022, "Enhanced Heat Transfer Performance of Multiple Triangular Air Flow Passages in Parallel With Inclined Fins for Flat Plate Solar Air Heater," ASME J. Sol. Energy Eng., **144**(5), p. 051003.
[8] Chhaparwal, G. K., Dayal, R., Goyal, R., and Srivastava, A., 2021, "Geometrical Optimization of a Smooth Solar Air Heater Duct," ASME J. Sol. Energy Eng., **143**(1), p. 011008.
[9] Jain, S. K., Agrawal, G. D., and Misra, R., 2020, "Experimental Investigation of Thermohydraulic Performance of the Solar Air Heater Having Arc-Shaped Ribs With Multiple Gaps," ASME J. Therm. Sci. Eng. Appl., **12**(1), p. 011014.
[10] Jain, S. K., Agrawal, G. D., and Misra, R., 2021, "Heat Transfer Augmentation Using Multiple Gaps in Arc-Shaped Ribs Roughened Solar Air Heater: An Experimental Study," Energy Sources, Part A Recover. Util. Environ. Eff., **43**(24), pp. 3345–3356.
[11] Jain, S. K., Agrawal, G. D., Misra, R., Verma, P., Rathore, S., and Jamuwa, D. K., 2019, "Performance Investigation of a Triangular Solar Air Heater Duct Having Broken Inclined Roughness Using Computational Fluid Dynamics," ASME J. Sol. Energy Eng., **141**(6), p. 061008.
[12] Jain, S. K., Misra, R., Kumar, A., and Agrawal, G. D., 2022, "Thermal Performance Investigation of a Solar Air Heater Having Discrete V-Shaped Perforated Baffles," Int. J. Ambient Energy, **43**(1), pp. 243–251.
[13] Jain, S. K., Agrawal, G. D., and Misra, R., 2019, "A Detailed Review on Various V-Shaped Ribs Roughened Solar Air Heater," Heat Mass Transfer, **55**(12), pp. 3369–3412.
[14] Kumar, V., 2019, "Nusselt Number and Friction Factor Correlations of Three Sides Concave Dimple Roughened Solar Air Heater," Renewble Energy, **135**, pp. 355–377.
[15] Promthaisong, P., and Eiamsa-ard, S., 2019, "Fully Developed Periodic and Thermal Performance Evaluation of a Solar Air Heater Channel With Wavy-Triangular Ribs Placed on an Absorber Plate," Int. J. Therm. Sci., **140**, pp. 413–428.
[16] Kumar, R., Kumar, A., and Goel, V., 2019, "Performance Improvement and Development of Correlation for Friction Factor and Heat Transfer Using Computational Fluid Dynamics for Ribbed Triangular Duct Solar Air Heater," Renewble Energy, **131**, pp. 788–799.
[17] Singh, S., Dhruw, L., and Chander, S., 2019, "Experimental Investigation of a Double Pass Converging Finned Wire Mesh Packed Bed Solar Air Heater," J. Energy Storage, **21**, pp. 713–723.
[18] Ahmad, I., Khan, N. H., Hassan, M. A., and Paswan, M. K., 2020, "Three-Dimensional Thermo-Hydraulic Analysis of Solar Air Heater With Equilateral Prism-Shaped Rib Roughness," ASME J. Sol. Energy Eng., **142**(5), p. 051001.
[19] Lee, A. H. I., Chen, H. H., and Kang, H. Y., 2009, "Multi-Criteria Decision Making on Strategic Selection of Wind Farms," Renewble Energy, **34**(1), pp. 120–126.
[20] Singh, T., Patnaik, A., and Chauhan, R., 2016, "Optimization of Tribological Properties of Cement Kiln Dust-Filled Brake Pad Using Grey Relation Analysis," Mater. Des., **89**, pp. 1335–1342.
[21] Ahlawat, V., Anuradha, P., and Kajal, S., 2021, "Preference Selection of Brake Friction Composite Using Entropy-VIKOR Technique," Mater. Today Proc., **46**(19), pp. 9573–9579.
[22] Zheng, G., and Wang, X., 2020, "The Comprehensive Evaluation of Renewable Energy System Schemes in Tourist Resorts Based on VIKOR Method," Energy, **193**, p. 116676.
[23] Mojaver, P., Khalilarya, S., and Chitsaz, A., 2020, "Multi-Objective Optimization and Decision Analysis of a System Based on Biomass Fueled SOFC Using Couple Method of Entropy/VIKOR," Energy Convers. Manage., **203**, p. 112260.
[24] Li, H., Wang, W., Fan, L., Li, Q., and Chen, X., 2020, "A Novel Hybrid MCDM Model for Machine Tool Selection Using Fuzzy DEMATEL, Entropy Weighting and Later Defuzzification VIKOR," Appl. Soft Comput. J., **91**, p. 106207.
[25] Chou, Y. C., Yen, H. Y., and Sun, C. C., 2014, "An Integrate Method for Performance of Women in Science and Technology Based on Entropy Measure for Objective Weighting," Qual. Quant., **48**(1), pp. 157–172.
[26] Das, S., Dhalmahapatra, K., and Maiti, J., 2020, "Z-Number Integrated Weighted VIKOR Technique for Hazard Prioritization and Its Application in Virtual Prototype Based EOT Crane Operations," Appl. Soft Comput. J., **94**, p. 106419.
[27] Demirel, H., Şener, B., Yildiz, B., and Balin, A., 2020, "A Real Case Study on the Selection of Suitable Roll Stabilizer Type for Motor Yachts Using Hybrid Fuzzy AHP and VIKOR Methodology," Ocean Eng., **217**, p. 108125.
[28] Narayanamoorthy, S., Geetha, S., Rakkiyappan, R., and Joo, Y. H., 2019, "Interval-Valued Intuitionistic Hesitant Fuzzy Entropy Based VIKOR Method for Industrial Robots Selection," Expert Syst. Appl., **121**, pp. 28–37.
[29] Rani, P., Mishra, A. R., Pardasani, K. R., Mardani, A., Liao, H., and Streimikiene, D., 2019, "A Novel VIKOR Approach Based on Entropy and Divergence

Measures of Pythagorean Fuzzy Sets to Evaluate Renewable Energy Technologies in India," J. Clean. Prod., **238**, p. 117936.
[30] Shemshadi, A., Shirazi, H., Toreihi, M., and Tarokh, M. J., 2011, "A Fuzzy VIKOR Method for Supplier Selection Based on Entropy Measure for Objective Weighting," Expert Syst. Appl., **38**(10), pp. 12160–12167.
[31] Sun, P., Liu, Y., Qiu, X., and Wang, L., 2015, "Hybrid Multiple Attribute Group Decision-Making for Power System Restoration," Expert Syst. Appl., **42**(19), pp. 6795–6805.
[32] Wang, L., Zhang, H. Y., Wang, J. Q., and Li, L., 2018, "Picture Fuzzy Normalized Projection-Based VIKOR Method for the Risk Evaluation of Construction Project," Appl. Soft Comput. J., **64**, pp. 216–226.
[33] Sharma, A., Chauhan, R., Singh, T., Kumar, A., Kumar, R., Kumar, A., and Sethi, M., 2017, "Optimizing Discrete V Obstacle Parameters Using a Novel Entropy-VIKOR Approach in a Solar Air Flow Channel," Renewble Energy, **106**, pp. 310–320.
[34] Gao, Z., Liang, R. Y., and Xuan, T., 2019, "VIKOR Method for Ranking Concrete Bridge Repair Projects With Target-Based Criteria," Results Eng., **3**, p. 100018.
[35] Duckstein, L., and Opricovic, S., 1980, "Multiobjective Optimization in River Basin Development," Water Resour. Res., **16**(1), pp. 14–20.
[36] Zeleny, M., 2011, "Multiple Criteria Decision Making (MCDM): From Paradigm Lost to Paradigm Regained?," J. Multi-Criteria Decis. Anal., **18**(1–2), pp. 77–89.
[37] Yu, P. L., 1973, "A Class of Solutions for Group Decision Problems," Manage. Sci., **19**(8), pp. 936–946.
[38] Umamaheswari, A., and Kumari, P., 2014, "Fuzzy TOPSIS and Fuzzy VIKOR Methods Using the Triangular Fuzzy Hesitant Sets," Int. J. Comput. Sci. Eng. Inf. Technol. Res., **4**(3), pp. 15–24.
[39] Standard, A.S.H.R.A.E., 93, 2003, "Method of Testing to Determine the Thermal Performance of Solar Collectors," American Society of Heating, Refrigeration and Air Conditioning Engineers, Atlanta, GA.
[40] Webb, R. L., and Eckert, E. R. G., 1972, "Application of Rough Surfaces to Heat Exchanger Design," Int. J. Heat Mass Transfer, **15**(9), pp. 1647–1658.
[41] Jain, S. K., Misra, R., and Agrawal, G. D., 2020, "Effect of Gap Width on Thermal Performance of Solar Air Heater Having Arc-Shaped Ribs With Symmetrical Gaps: An Experimental Investigation," Environ. Dev. Sustainable, **22**(7), pp. 6563–6583.